Smaller than a nanoparticle with the design of discrete polynuclear molecular complexes displaying near-infrared to visible upconversion

Journal:	*Dalton Transactions*
Manuscript ID:	DT-ART-08-2014-002336.R1
Article Type:	Paper
Date Submitted by the Author:	18-Sep-2014
Complete List of Authors:	Piguet, Claude; Sciences II, Departement of Inorganic Analytical Chemistry Zare, Davood; University of Geneva, Inorganic Chemistry Suffren, Yan; University of Geneva, Physical Chemistry Guénée, Laure; University of Geneva, CHIAM Eliseeva, Svetlana; Centre de Biophysique Moléculaire CNRS, Nozary, Homayoun; University of Geneva, Inorganic chemistry Aboshyan-Sorgho, Lilit; University of Geneva, Inorganic Chemistry Petoud, Stephane; CNRS, Centre de Biophysique Moléculaire; University of Pittsburgh, Department of Chemistry Hauser, Andreas; Unniversity of Geneva, Physical Chemistry

Smaller than a nanoparticle with the design of discrete polynuclear molecular complexes displaying near-infrared to visible upconversion.[†]

Davood Zare,[⊥] Yan Suffren,[§] Laure Guénée,[#] Svetlana V. Eliseeva,[±] Homayoun Nozary,[⊥] Lilit Aboshyan-Sorgho,[⊥] Stéphane Petoud,[±,*] Andreas Hauser,[§,*] and Claude Piguet[⊥,*]

[⊥] *Department of Inorganic and Analytical Chemistry, University of Geneva, 30 quai E. Ansermet, CH-1211 Geneva 4, Switzerland. E-mail:* Claude.Piguet@unige.ch

[§] *Department of Physical Chemistry, University of Geneva, 30 quai E. Ansermet, CH-1211 Geneva 4, Switzerland. E-mail:* Andreas.Hauser@unige.ch

[#] *Laboratory of Crystallography, University of Geneva, 24 quai E. Ansermet, CH-1211 Geneva 4, Switzerland.*

[±] *Centre de Biophysique Moléculaire, CNRS UPR 4301, Rue Charles Sadron, F-45071 Orléans Cedex 2, France. E-mail:* Stephane.Petoud@inserm.fr

Submitted to Dalton Transactions dedicated themed issue: Advancing the chemistry of the f-elements

---

[†] Electronic Supplementary Information (ESI) available. For ESI see DOI: xxx.

Abstract

This work shows that the operation of near-infrared to visible light-upconversion in a discrete molecule is not limited to non-linear optical processes, but may result from superexcitation processes using linear optics. The design of nine-coordinate metallic sites made up of neutral *N*-heterocyclic donor atoms in the kinetically inert dinuclear $[GaEr(\mathbf{L1})_3]^{6+}$ and trinuclear $[GaErGa(\mathbf{L2})_3]^{9+}$ helicates leads to $[ErN_9]$ chromophores displaying unprecedented dual visible nanosecond $Er(^4S_{3/2}\rightarrow{}^4I_{15/2})$ and near-infrared microsecond $Er(^4I_{13/2}\rightarrow{}^4I_{15/2})$ emissive components. Attempts to induce one ion excited-state absorption (ESA) upconversion upon near-infrared excitation of these complexes failed because of the too faint Er-centred absorption cross sections. The replacement of the trivalent gallium cation with a photophysically-tailored pseudo-octahedral $[CrN_6]$ chromophore working as a sensitizer for trivalent erbium in $[CrEr(\mathbf{L1})_3]^{6+}$ improves the near-infrared excitation efficiency leading to the observation of a weak energy transfer upconversion (ETU). The connection of a second sensitizer in $[CrErCr(\mathbf{L2})_3]^{9+}$ generates a novel mechanism for upconversion, in which the superexcitation process is based on the Cr^{III}-sensitizers. Two successive Cr→Er energy transfer processes (concerted-ETU) compete with standard Er-centred ETU, and a gain in upconverted luminescence by a factor larger than statistical values is predicted and observed.

Introduction

Compared to the classical spontaneous transformation of energy in physics (energy degradation) and in chemistry (spontaneous chemical reactions induced by negative free energy changes), near-infrared (NIR) to visible light-upconversion processes may appear puzzling. However, it has been known for a long time that the intense electromagnetic irradiation (typically in the range of $MW\cdot cm^{-2}$) of polarizable materials may induce weak non-linear responses, which ultimately produce photons of higher energy than those used for the excitation.[1] Despite the low quantum yields of such non-linear processes, the transparency of living tissues to incident NIR light was attractive enough to exploit these phenomena for the *in vivo* sensitization of optical probes and sensors in photobiology.[2] For technological applications, such huge input intensities are of limited interest and efforts are directed towards the design of upconverting materials based on linear optical processes and compatible with common light sources, for instance for the conversion of the NIR part of the solar light into green emission compatible with its absorption by dye-sensitized or by crystalline silica solar cells (the power-density of the terrestrial solar irradiance is approximately 0.1 W·cm^{-2}).[3]

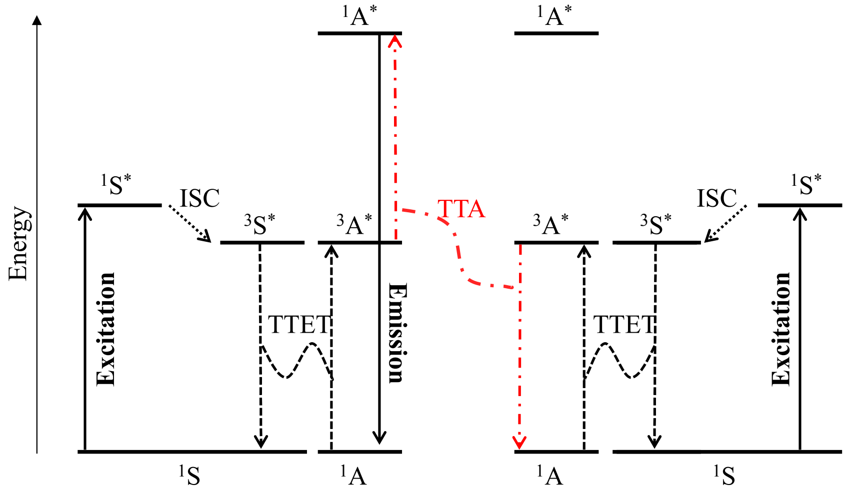

Scheme 1 Qualitative Jablonski diagram illustrating the sensitized triplet-triplet annihilation (TTA) upconversion process operating in a S/A mixture. Solid arrows indicate transitions in which a photon is involved, while black dashed arrows indicate radiationless processes (ISC = intersystem crossing and TTET = triplet-triplet energy transfer). The alternating dashed-dotted red arrows stand for the triplet-triplet annihilation mechanism.

In this context, the non-coherently sensitized upconversion based on triplet-triplet annihilation (TTA) is currently one of the most efficient strategies.[4] According to the mechanism depicted in Scheme 1, a sensitizer (S)/acceptor (A) pair of molecules is required. The sensitizer S is responsible for the $^1S \rightarrow {}^1S^*$ light-harvesting process which is followed by an intersystem crossing (ISC) process leading to the establishment of a long-lived triplet excited state $^3S^*$. The subsequent $^3S^*/^1A \rightarrow {}^1S/^3A^*$ Dexter-type triplet-triplet energy transfer provides an acceptor-centred triplet state $^3A^*$, which is sufficiently long-lived to diffuse and to collide with a second partner. The triplet-triplet annihilation then produces a mixture of singlet, triplet and quintet excited dimers, in which the $^3A^*$

+ $^{3}\mathrm{A}^{*} \rightarrow {}^{1}\mathrm{A}^{*} + {}^{1}\mathrm{A}$ pathway leads to the targeted high-energy singlet excited state on the acceptor. Relaxation of the $^{1}\mathrm{A}^{*}$ state to the ground state is finally accompanied by the emission of a photon of higher energy than those involved in the excitation process. Typical green-to-blue upconversion is experimentally observed by using sensitizers and activators containing aromatic ring systems of various sizes. However, the requirements for the diffusion and collision of two excited triplet acceptors for TTA limits this methodology to intermolecular processes occurring in solution, in rubbery polymeric materials or in solid matrices ensuring sufficiently efficient diffusion of molecules and/or molecular excitons under anaerobic conditions (since dioxygen can easily quench triplet excited states).[4]

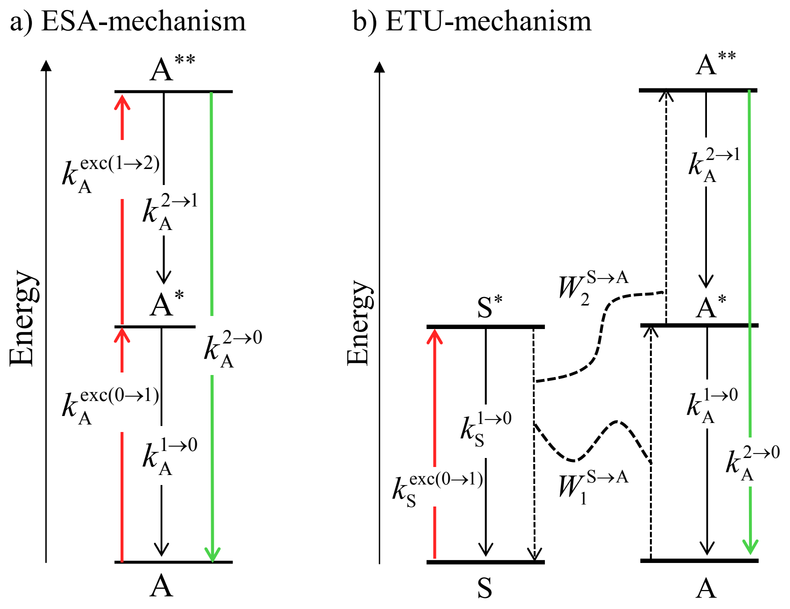

Scheme 2 Kinetic schemes depicting the modelling of activator-centred superexcitation processes according to a) a one ion excited state absorption (ESA) process and b) an energy transfer upconversion (ETU) process occurring upon off-resonance excitations. $k_{\mathrm{A}}^{\mathrm{exc}(0\to1)}$ and $k_{\mathrm{S}}^{\mathrm{exc}(0\to1)}$ are the pumping rate constants for the irradiation into the activator, respectively sensitizer absorption bands, $k_{\mathrm{A}}^{i\to j}$ and $k_{\mathrm{S}}^{i\to j}$ are the decay rate constants (i.e. the sum of radiative and non-radiative processes) of level i into level j centred on the sensitizer and on the activator, respectively. $W_{n}^{\mathrm{S}\to\mathrm{A}}$ are the rate constants of sensitizer-to-activator energy transfer processes. Red solid arrows correspond to excitation photons and green solid arrows stand for upconverted emission.

Though less efficient in term of quantum yields, the superexcitation mechanisms depicted in Scheme 2 also rely on linear and sequential optical processes. They are currently implemented in low-phonon nanoparticles,[5] but their engineering can be theoretically further miniaturized and confined in a single molecular entity. For the one ion excited state absorption mechanism (ESA, Scheme 2a), the initial excitation produces an intermediate excited state, the lifetime of which must be long enough to allow for a second absorption process to occur. Such a situation is difficult to implement in molecules where the existence of high-energy oscillators drastically reduces the excited-state lifetimes.[6] Indeed, attempts to detect ESA-processes in coordination complexes using trivalent lanthanides as activators (Ln = Er, Tm, Yb) failed to date,[7] except for a very recent report claiming that NIR to visible ESA-upconversion could be detected upon very intense irradiation of dimethysulfoxide solutions containing Tm^{3+}.[8] Indirect excitation using sensitizers for collecting the initial NIR irradiation followed by energy transfer onto the acceptor (ETU, Scheme 2b) may benefit from the larger absorption cross sections and longer lifetimes of the sensitizers,[5] but to date only little attention has been given to the implementation of ETU in molecules. In 2003, Hoshino and coworkers reported a surprising linear Er-centred upconversion process induced by the intense irradiation of the low-energy tail of the ligand-absorption band in films of $[Er(quinolinate)_3]$ complexes, but its alternative assignment to a ligand-centred non-linear optical two-photon absorption followed by Er-centred luminescence could not be excluded.[9] Inspired by this pioneering work, Piguet and co-workers used trivalent chromium for the indirect sensitization of Er^{III} in the trinuclear triple-stranded $[CrErCr(\mathbf{L2})]^{9+}$ helicate.[10] Continuous-wave NIR irradiation at 750 nm indeed generated the excitation of the chromium cations *via* their spin-flip $Cr(^2E \leftarrow {}^4A_2)$ and $Cr(^2T_1 \leftarrow {}^4A_2)$ transitions, which were responsible for a weak, but reproducible green upconverted erbium-centred $Er(^4S_{3/2} \rightarrow {}^4I_{15/2})$ luminescence at 540 nm (Scheme 3).[10] The quadratic dependence of the upconverted emission upon incident intensity observed in diluted solutions, combined with the crucial role played by Cr→Er energy transfer processes unambiguously support the presence of an ETU mechanism operating within a single supramolecular complex.[11]

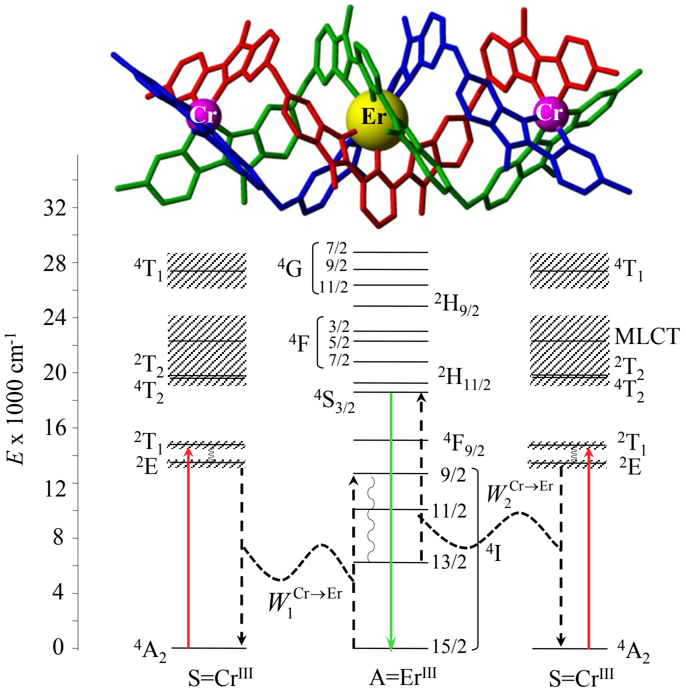

Scheme 3 Jablonski diagrams obtained from absorption and emission spectra recorded for the different chromophores in [CrErCr(**L2**)$_3$](CF$_3$SO$_3$)$_9$. Black dashed arrows indicate radiationless sensitizer-to-activator energy transfer processes and curled arrows stand for non-radiative internal conversion. Red solid arrows correspond to the NIR excitation photons and the green solid arrow stands for the visible upconverted emission. Adapted from ref. 11.

Further optimization requires a deeper level of understanding of the ETU mechanism in [CrErCr(**L2**)]$^{9+}$. This work can be achieved thanks to the preparation of analogous complexes, in which (i) the photophysically active Cr^{III} and Er^{III} chromophores are replaced by ‘innocent’ partners and (ii) the number of Cr-sensitizers per Er-activators is stepwise increased from 0 to 2. Here we thus report on the chemical strategy used for the design of isostructural polynuclear heterometallic gallium-lanthanide and chromium-lanthanide complexes, in which energy transfer upconversion can be deciphered and optimized.

Results and discussion

Optimizing the erbium coordination sphere for its use as an activator in molecular upconversion processes. Except for the report of Hoshino and co-workers, who assigned not less than ten emission bands to Er-centred luminescence upon ligand excitation in the [Er(quinolinate)$_3$]

complexes,[9] a behaviour that is reminiscent to that found for Er-doped solids,[12] we are not aware of the description of any erbium coordination complex displaying other luminescence signal than the 1.5 µm band attributed to the Er($^4I_{13/2} \rightarrow {}^4I_{15/2}$) transition.[13] This observation agrees with the large weighted average effective vibrational energy of ~2000 cm^{-1} participating in non-radiative relaxation processes for lanthanide complexes containing organic ligands.[7] For Er^{III}, the reduced energy gap *p* (in phonons units) between adjacent levels hardly exceeds $p = 2$ and the dominant nonradiative relaxation prevents luminescence in coordination complexes, except for the fluorescence of the lowest Er($^4I_{13/2}$) excited state for which $p \geq 3$.[7]

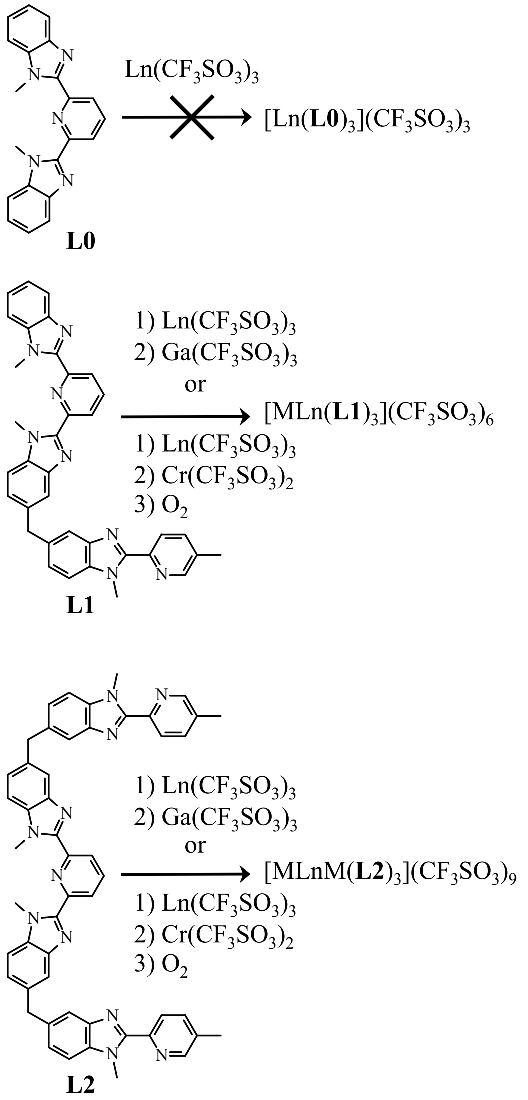

Scheme 4. Chemical structures of ligands **L0**-**L2** and preparation of the dinuclear [MLn(**L1**)$_3$](CF$_3$SO$_3$)$_6$ and trinuclear [MLnM(**L1**)$_3$](CF$_3$SO$_3$)$_9$ helicates (M = Ga, Cr and Ln = Ho, Er, Tm, Y)

Efforts made for protecting the erbium-activator from high-energy C-H oscillators in coordination complexes succeeded in extending the Er($^4I_{13/2}$) excited state lifetimes by more than one order of magnitude,[13i] and we therefore planned to take advantage of this strategy with the introduction of rigid unsaturated bis-(*N*-methyl-benzimidazol-2-yl)pyridine tridentate units **L0** into the segmental ligands **L1** and **L2** (Scheme 4, see Appendix 1 in the ESI). Reaction of **L0** with Ln(CF_3SO_3)$_3$ was known to give poorly stable triple-helical [Ln(**L0**)$_3$]$^{3+}$ complexes with the small Y^{3+} and Er^{3+} cations,[14] but the formation of these [LnN$_9$] chromophores was favoured by the self-assembly of **L1** and **L2** with Ln(CF_3SO_3)$_3$ in the presence of Ga(CF_3SO_3)$_3$. The heterometallic dinuclear [GaLn(**L1**)$_3$](CF_3SO_3)$_6$·*m*C_2H_5CN·*n*H_2O and trinuclear [GaLnGa(**L2**)$_3$](CF_3SO_3)$_9$·*m*C_2H_5CN·*n*H_2O helicates could be isolated in 40-90% yields (Scheme 4 and Table S1 in the ESI).

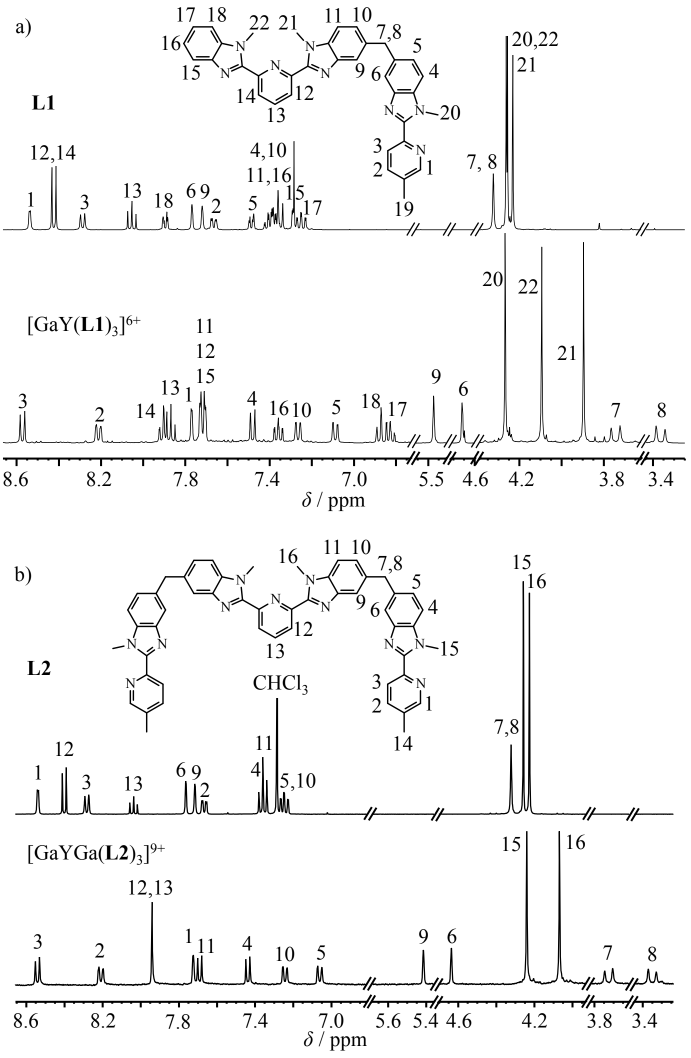

Figure 1 ^1H NMR spectra with assignment for a) **L1** and [GaY(**L1**)$_3$]$^{6+}$ and b) **L2** and [GaYGa(**L2**)$_3$]$^{9+}$ at 293 K (in $CDCl_3$ for the ligands and in CD_3CN for the complexes).

ESI-MS data unambiguously establish the charge balance $[\mathrm{GaLn}(\mathbf{L1})_3]^{6+}/6\mathrm{CF_3SO_3^-}$ and $[\mathrm{GaLnGa}(\mathbf{L2})_3]^{9+}/9\mathrm{CF_3SO_3^-}$ (Tables S2-S3 in the ESI) whereas the ^{1}H NMR spectra collected for the diamagnetic $\mathrm{Ga^{3+}/Y^{3+}}$ pair in acetonitrile at submillimolar concentrations confirmed the self-assembly of stable C_3-symmetrical $[\mathrm{GaY}(\mathbf{L1})_3]^{6+}$ (Figure S1 in the ESI) and D_3-symmetrical $[\mathrm{GaYGa}(\mathbf{L2})_3]^{9+}$ complexes (Figure S2 in the ESI), for which the unusual upfield chemical shifts of the aromatic protons H6 and H9 together with the diastereotopic splitting of H7 and H8 were diagnostic for the twisted arrangement of the ligand strands in these triple-stranded helicates (Figure 1).[15] Upon addition of one equivalent of paramagnetic $\mathrm{Eu(CF_3SO_3)_3}$ into an acetonitrile solution of $[\mathrm{GaYGa}(\mathbf{L2})_3]^{9+}$, the ^{1}H NMR spectrum remained unchanged for months at room temperature, thus demonstrating the exceptional kinetic inertness of these trinuclear helicates (Figure S3 in the ESI). In contrast, the trivalent lanthanide coordinated in the dinuclear $[\mathrm{GaY}(\mathbf{L1})_3]^{6+}$ complex was more accessible to metal exchange and the replacement of $\mathrm{Y^{3+}}$ with $\mathrm{Eu^{3+}}$ according to the equilibrium (1) could be monitored on the timescale of hours (Figure 2 and Figure S4 in the ESI).

$$[\mathrm{GaY}(\mathbf{L1})_3]^{6+} + \mathrm{Eu^{3+}} \rightleftharpoons [\mathrm{GaEu}(\mathbf{L1})_3]^{6+} + \mathrm{Y^{3+}} \qquad K_{\mathrm{exch}}^{\mathrm{Y,Eu}} \tag{1}$$

$$K_{\mathrm{exch}}^{\mathrm{Y,Eu}} = \frac{\beta_{1,1,3}^{\mathrm{Ga,Eu,}\mathbf{L1}}}{\beta_{1,1,3}^{\mathrm{Ga,Y,}\mathbf{L1}}} = \frac{[\mathrm{GaEu}]_{\mathrm{eq}}[\mathrm{Y}]_{\mathrm{eq}}}{[\mathrm{GaY}]_{\mathrm{eq}}[\mathrm{Eu}]_{\mathrm{eq}}} \tag{2}$$

The integration of the ^{1}H NMR signals at chemical equilibrium gave $K_{\mathrm{exch}}^{\mathrm{Y,Eu}} = 134(3)$ according to eq. (2), from which a stabilization factor of $\xi = \log\left(K_{\mathrm{exch}}^{\mathrm{Y,Eu}}\right) = \log\left(\beta_{1,1,3}^{\mathrm{Ga,Eu,}\mathbf{L1}}\right) - \log\left(\beta_{1,1,3}^{\mathrm{Ga,Y,}\mathbf{L1}}\right) = 2.13(1)$ was deduced for the replacement of a small $\mathrm{Y^{3+}}$ with a midrange size $\mathrm{Eu^{3+}}$ cation in the nine-coordinate cavity found in $[\mathrm{GaLn}(\mathbf{L1})_3]^{6+}$. The $\beta_{1,1,3}^{\mathrm{Ga,Ln,}\mathbf{L1}}$ stand for the cumulative formation constants of the $[\mathrm{GaLn}(\mathbf{L1})_3]^{6+}$ complexes, while $[\mathrm{GaLn}]_{\mathrm{eq}}$ and $[\mathrm{Ln}]_{\mathrm{eq}}$ correspond to the equilibrium concentrations of complexes and free metals (a standard concentration $c^{\theta} = 1.0$ M is taken for the reference state, see Appendix 2 in the ESI). This trend is remarkable when one considers the minute $\Delta R_{\mathrm{CN=9}}^{\mathrm{Y\rightarrow Eu}} = 0.045$ Å increase in the lanthanide nine-coordinate ionic radius, but it is in line with $\xi = 1.3(2)$ reported for the replacement of Ln = $\mathrm{Ho^{3+}}$ with Ln = $\mathrm{Gd^{3+}}$ in $[\mathrm{Ln}(\mathbf{L0})_3]^{3+}$($\Delta R_{\mathrm{CN=9}}^{\mathrm{Ho\rightarrow Gd}} = 0.035$

Å).[14c] Since no significant quantity of intermediate complexes could be detected by ^{1}H NMR during the exchange reaction (Figure S4), reaction (1) could be tentatively considered as a reversible second-order elementary reaction, for which the quadratic rate law is given by

$$-\frac{d[\mathrm{GaY}]}{dt} = [\mathrm{GaY}]^2\left(k_f - k_r\right) + [\mathrm{GaY}]\left\{k_f\left([\mathrm{Eu}]_{\mathrm{tot}} - [\mathrm{Ga}]_{\mathrm{tot}}\right) + k_r\left([\mathrm{Y}]_{\mathrm{tot}} + [\mathrm{Ga}]_{\mathrm{tot}}\right)\right\} - k_r[\mathrm{Ga}]_{\mathrm{tot}}[\mathrm{Y}]_{\mathrm{tot}} \quad (3)$$

where k_f and k_r stand for the forward, respectively backward second-order rate constants (see Appendix 3 in the ESI).[16] However, the observation of a mono-exponential kinetic traces for both [GaY] depletion and [GaEu] rising with a common rate constant $k = 2.3(1)\cdot10^{-5}$ s^{-1} ($\tau_{1/2} = \ln(2)/k$ = 8.3(4) hours, Figure 2) suggests the more complicated mechanism shown in eq. (4), in which the first-order dissociation processes characterized by k_1 and k_{-2} values are the rate limiting steps.[17]

$$\left[\mathrm{GaY}(\mathbf{L1})_3\right]^{6+} + \mathrm{Eu}^{3+} \xrightleftharpoons[k_{-1}]{k_1} \left[\mathrm{Ga}(\mathbf{L1})_3\right]^{3+} + \mathrm{Y}^{3+} + \mathrm{Eu}^{3+} \xrightleftharpoons[k_{-2}]{k_2} \left[\mathrm{GaEu}(\mathbf{L1})_3\right]^{6+} + \mathrm{Y}^{3+} \quad (4)$$

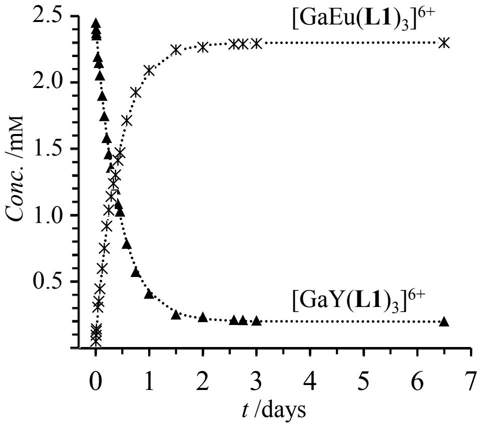

Figure 2 Kinetic traces monitored by ^{1}H NMR for the reaction of [GaY(**L1**)$_3$](CF$_3$SO$_3$)$_6$ (1.0 eq) with Eu(CF$_3$SO$_3$)$_3$ (1.0 eq) at 293 K. The dotted lines correspond to the best exponential fits.

We conclude that the non-covalent cryptate [GaYGa(**L2**)$_3$]$^{9+}$ is sufficiently inert ($\tau_{1/2}$ > 1 month) to be used as a host matrix for diluting isomorphous and photophysically active [GaErGa(**L2**)$_3$]$^{9+}$, [CrYCr(**L2**)$_3$]$^{9+}$ or [CrErCr(**L2**)$_3$]$^{9+}$ complexes using co-crystallization. On the contrary, [GaY(**L1**)$_3$]$^{6+}$ is too labile ($\tau_{1/2}$ = 8.3(4) hours) for accommodating [CrEr(**L1**)$_3$]$^{6+}$ guests without undergoing lanthanide exchange processes.

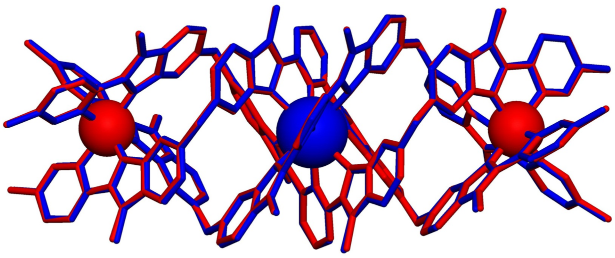

Figure 3 Superimposition of the molecular structures of [GaErGa(**L2**)$_3$]$^{9+}$ (red) and [CrEuCr(**L2**)$_3$]$^{9+}$ (blue) observed in the crystal structures of [GaErGa(**L2**)$_3$](CF$_3$SO$_3$)$_9$(CH$_3$CN)$_{35.5}$ and [CrEuCr(**L2**)$_3$](CF$_3$SO$_3$)$_9$(C$_2$H$_5$CN)$_{30}$.[10] The hydrogen atoms are omitted for clarity.

Slow diffusion of tert-butylmethylether into an acetonitrile solution of [GaErGa(**L2**)$_3$]$^{9+}$ provided prisms of [GaErGa(**L2**)$_3$](CF$_3$SO$_3$)$_9$(CH$_3$CN)$_{35.5}$, the crystal structure of which (Figure S5) is isostructural with those reported for[CrLnCr(**L2**)$_3$](CF$_3$SO$_3$)$_9$(C$_2$H$_5$CN)$_{30}$ (Ln = Eu, Yb, Figure 3 and Table S4).[10] The close packing of the triple-helical cations [GaErGa(**L2**)$_3$]$^{9+}$ in the crystal produces large interstitial cavities, which are filled with disordered counter-anions and solvent molecules (Figures S6-S7). The erbium atom is coordinated by nine heterocyclic nitrogen atoms occupying the vertices of a distorted tricapped trigonal prism. We were unable to obtain X-ray quality crystals for [GaEr(**L1**)$_3$](CF$_3$SO$_3$)$_6$, but the slow diffusion of tert-butylmethylether into a concentrated propionitrile solution of [CrEr(**L1**)$_3$]$^{6+}$ succeeded in crystallizing the analogous dinuclear [CrEr(**L1**)$_3$](CF$_3$SO$_3$)$_6$(C$_3$H$_5$N)$_{26}$ complex. The [CrEr(**L1**)$_3$]$^{6+}$ cations are packed in columns with opposite helicities along the crystallographic threefold axes passing through the metal ions (Figure 4a, Figure S8 and Table S5). In line with the rigidity of the polyaromatic strands, the intermetallic distance Cr···Er = 8.704(1) Å found in [CrEr(**L1**)$_3$]$^{6+}$ compares well with those found in the trinuclear analogue (Ga1···Er1 = 8.974(1) Å and Er1···Ga2 = 8.887(1)Å). The superimposition of the triple-helical cations [CrEr(**L1**)$_3$]$^{6+}$ with [GaErGa(**L2**)$_3$]$^{9+}$ further demonstrates similar triple-helical organizations (Figure 4b).

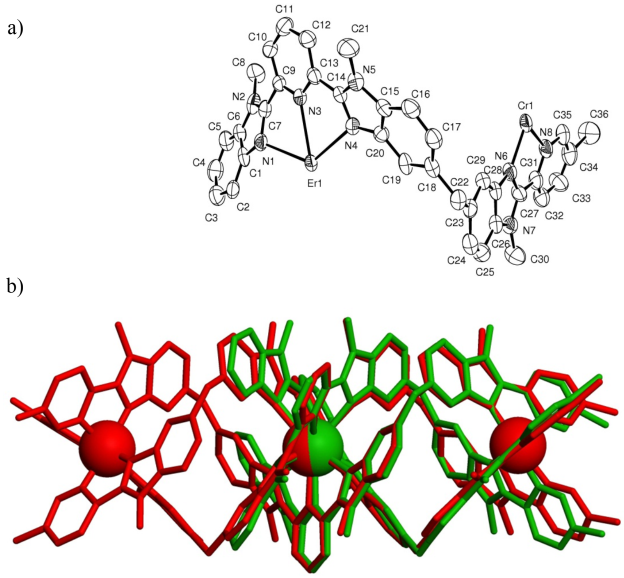

Figure 4 a) ORTEP view with the numbering scheme of the asymmetric unit in the crystal structure of [CrEr(**L1**)$_3$](CF$_3$SO$_3$)$_6$(C$_3$H$_5$N)$_{26}$. Ellipsoids are represented at the 30% probability level and hydrogen atoms are omitted for clarity. b) Superimposition of the molecular structures of [CrEr(**L1**)$_3$]$^{6+}$ (green) and [GaErGa(**L2**)$_3$]$^{9+}$ (red).

The photophysical properties confirmed the structural similarities, and ligand-centred excitation at λ_{ex} = 405 nm ($\tilde{\nu}_{exc}$ = 24691 cm^{-1}) of solid-state samples of [GaEr(**L1**)$_3$](CF$_3$SO$_3$)$_6$ and [GaErGa(**L2**)$_3$](CF$_3$SO$_3$)$_9$ displayed standard Ligand-to-Erbium energy transfer followed by NIR emission signals centred at 6500 cm^{-1} assigned to the split Er($^4I_{13/2}\rightarrow{}^4I_{15/2}$) transition.[11] The roughly temperature-independent mono-exponential lifetimes found for the Er($^4I_{13/2}$) excited state (3.1(4) µs for GaEr and 4.1(3) µs for GaErGa between 10-293 K, entries 3-4 in Table 1 and Figure S9) combined with the detection of additional green Er($^4S_{3/2}\rightarrow{}^4I_{15/2}$) emission centred at λ_{em} = 542 nm in both complexes ($\tilde{\nu}_{em}$ = 18450 cm^{-1}, Figures 5a and S10) reflect the exceptional protection of the erbium cation from interactions with high-energy phonons and vibrations in these [ErN$_9$] chromophores.[11,18] Though technically challenging (see experimental section), the kinetic traces of the Er-centred green luminescence could be separated from the broad ligand-centred $\pi^*\rightarrow\pi$ emission and provided mono-exponential decay values with characteristic Er($^4S_{3/2}$) lifetimes of 38(4) ns for GaEr and 40(2) ns for GaErGa at 3K in the solid state (entries 5 and 6 in Table 1, Figure 5b and S11).

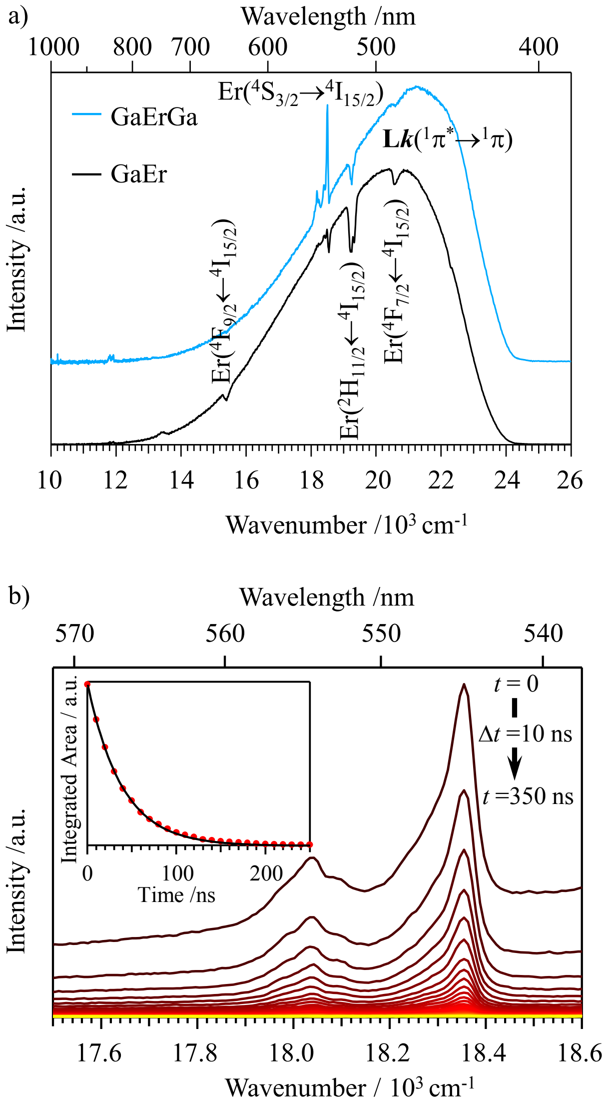

Figure 5 a) Luminescence spectra recorded for [GaEr(**L1**)$_3$](CF$_3$SO$_3$)$_6$ (black trace) and [GaErGa(**L2**)$_3$](CF$_3$SO$_3$)$_9$ (blue trace) at 3K in the solid state (λ_{ex} = 405 nm or $\tilde{\nu}_{exc}$ = 24691 cm^{-1}, cutoff filter 420 nm). The dips correspond to internal Er-centred re-absorption of ligand-centred emission.[13g] b) Time-resolved luminescence spectra recorded between t = 0 and t = 350 ns (Δt = 10 ns) and luminescence decay trace (inset) recorded for the Er($^4S_{3/2}\rightarrow{}^4I_{15/2}$) transition in [GaErGa(**L2**)$_3$](CF$_3$SO$_3$)$_9$ at 3K in the solid state (λ_{ex} = 355 nm or $\tilde{\nu}_{exc}$ = 24691 cm^{-1}, cutoff filter 420 nm). The black curve corresponds to the best exponential fit applied to the decay points deduced from the integration of the intensity traces of the Er($^4S_{3/2}\rightarrow{}^4I_{15/2}$) transition.

In conclusion, the tight wrapping of the three bulky polyaromatic *N*-heterocyclic tridentate binding units in the triple-helical [GaLn(**L1**)$_3$](CF$_3$SO$_3$)$_6$ and [GaLnGa(**L2**)$_3$](CF$_3$SO$_3$)$_9$ complexes produces compact, stable and inert nine-coordinate cavities for the lanthanide cations. For Ln = Er, the concomitant existence of a comparatively long-lived intermediate Er($^4I_{13/2}$) excited state and of a short-lived, but emissive Er($^4S_{3/2}$) excited state at higher-energy fulfils the two conditions required for the implementation of ETU in Er-containing molecular systems (Scheme 3). In a control experiment, direct continuous-wave laser excitation of the Er($^4I_{9/2}\leftarrow{}^4I_{15/2}$) transition centred at λ_{exc} = 647 nm ($\tilde{\nu}_{exc}$ = 15454 cm^{-1}) failed to induce upconverted signals in the Ga/Er complexes (Figure S12), which (i) confirmed Güdel's conclusion that there was little chance to detect single ion ESA in these molecular complexes,[7] and (ii) demonstrated that ligand-centred non-linear two-photon absorption processes did not compete efficiently with ETU in these conditions.

Optimizing the chromium coordination sphere for its use as a sensitizer in ETU processes with erbium activator. Based on the specific photophysical properties of the Er^{III} activator implemented in [MEr(**L1**)$_3$](CF$_3$SO$_3$)$_6$ and [MErM(**L2**)$_3$](CF$_3$SO$_3$)$_9$, the associated M sensitizers should fit the following criteria: 1) replace Ga^{III} in order to yield structurally-similar, kinetically inert and thermodynamically stable pseudo-octahedral [MN$_6$] coordination building block, 2) possess a sensitizing excited state, the energy of which is in close resonance with one of the Er-centred excited state for maximizing M→Er energy transfer processes and 3) display a transparent optical window centred around 18450 cm^{-1} in order to avoid the quenching by non-radiative energy transfer processes of the target upconverted emission arising from the Er($^4S_{3/2}$) excited state.[11] Altogether, the trivalent chromium with its [Ar]3d^3 electronic configuration is a promising candidate since the energies of its six lower excited levels can be tuned by the ligand-field strength (measured by Δ in pseudo-octahedral complexes) and by the nephelauxetic effect (measured by the reduction of the Racah parameters B and C for electron-electron repulsion) produced by the terminal didentate benzimidazole-2-yl-pyridine binding units involved in the [CrN$_6$] chromophores in [CrLn(**L1**)$_3$](CF$_3$SO$_3$)$_6$ and [CrLnCr(**L2**)$_3$](CF$_3$SO$_3$)$_9$ (eqs S1-S6 in Figure S13).[6] However, Cr^{III} is too inert to be used in a self-assembly process, and we therefore resorted to more labile Cr^{II} precursors followed by outer-sphere dioxygen oxidation for synthesizing [CrLn(**L1**)$_3$](CF$_3$SO$_3$)$_6$ and [CrLnCr(**L2**)$_3$](CF$_3$SO$_3$)$_9$ (Ln = Y, Er) complexes in 80-90% yields (Scheme 3 and Table S1-

S3). Orange X-ray quality prisms of [CrYCr(**L2**)$_3$](CF$_3$SO$_3$)$_9$ were found to be isostructural with [GaErGa(**L2**)$_3$](CF$_3$SO$_3$)$_9$, [GaYGa(**L2**)$_3$](CF$_3$SO$_3$)$_9$, [CrEuCr(**L2**)$_3$](CF$_3$SO$_3$)$_9$ and [CrYbCr(**L2**)$_3$](CF$_3$SO$_3$)$_9$.[11] The detailed analyses of the absorption and emission spectra recorded for [CrY(**L1**)$_3$](CF$_3$SO$_3$)$_6$ and [CrYCr(**L2**)$_3$](CF$_3$SO$_3$)$_9$ with the help of eqs S1-S6 gave Δ = 20130 cm^{-1}, B = 665 cm^{-1} and C = 2876 cm^{-1} for Cr^{3+} coordinated in the dinuclear complex, and Δ = 19940 cm^{-1}, B = 736 cm^{-1} and C = 2737 cm^{-1} for Cr^{3+} in the trinuclear helicate (Figure S13). These parameters are comparable to those found for pseudo-octahedral strong-field [Cr(2,2'-bipyridine)$_3$]$^{3+}$ (Δ = 23240 cm^{-1}, B = 761 cm^{-1} and C = 3044 cm^{-1}),[6] which indicates close locations of the didentate benzimidazole-pyridine and 2,2'-bipyridine binding units in the spectrochemical and nephelauxetic series.

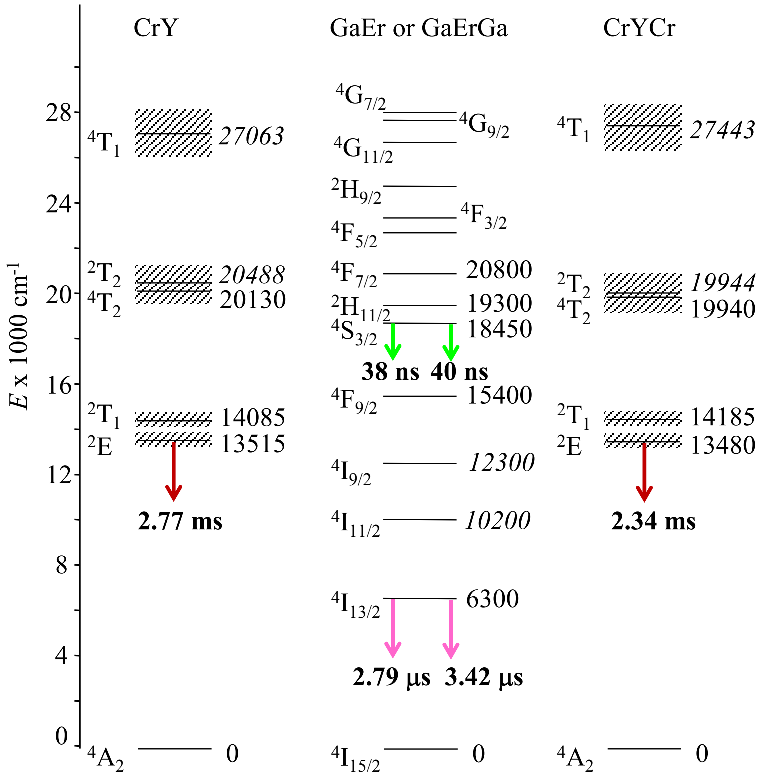

Figure 6 Jablonski diagrams for the [CrN$_6$] chromophores in [CrY(**L1**)$_3$](CF$_3$SO$_3$)$_6$ (left hand side) and in [CrYCr(**L2**)$_3$](CF$_3$SO$_3$)$_9$ (right-hand side) and for the [ErN$_9$] chromophores in [GaEr(**L1**)$_3$](CF$_3$SO$_3$)$_6$ and [GaErGa(**L2**)$_3$](CF$_3$SO$_3$)$_9$ (centre). The energies of the excited levels deduced from the absorption, excitation and emission spectra are given with normal fonts, while the value obtained by computing are given in italics. The emissive levels are shown with full downward arrows mentioning their characteristic lifetimes in pure solids at 3-10K.[11]

The complete energy level diagram built for the [CrN_6] and [ErN_9] chromophores in Figure 6 shows (i) a good match between the energy levels of the chromium sensitizer and those of the erbium activator for implementing efficient $Cr(^2E)\rightarrow Er(^4I_{9/2})$ energy transfer processes in the target [CrEr(**L1**)$_3$](CF_3SO_3)$_6$ and [CrErCr(**L2**)$_3$](CF_3SO_3)$_9$ helicates, (ii) large $Cr(^4T_2)$-$Cr(^2T_1)$ energy gaps compatible with the unquenched emission arising from the final $Er(^4S_{3/2})$ level and (iii) long luminescence lifetimes for the intermediate $Cr(^2E)$ and $Er(^4I_{13/2})$ levels involved in the planned ETU process (Scheme 3). As expected, continuous-wave laser excitation of the $Cr(^2E,^2T_1\leftarrow{}^4A_2)$ transitions in the control compounds [CrY(**L1**)$_3$](CF_3SO_3)$_6$ and [CrYCr(**L2**)$_3$](CF_3SO_3)$_9$ ($700 \leq \lambda_{exc} \leq 750$ nm, $13330 \leq \tilde{\nu}_{exc} \leq 14280$ cm^{-1}) failed to induce upconverted signals (Figure S16a), which excludes the possibilities of Cr-centred upconversion processes or spurious ETU from impurities.[19]

Combining chromium sensitizers with erbium activators for the implementation of ETU processes in molecular complexes. In the triple-stranded dinuclear [CrEr(**L1**)$_3$](CF_3SO_3)$_6$ and trinuclear [CrErCr(**L2**)$_3$](CF_3SO_3)$_9$ complexes, the optimized nine-coordinated pseudo-tricapped [ErN_9] chromophore is located at *ca* 9 Å from one (dinuclear CrEr) or two (trinuclear CrErCr) strong-field [CrN_6] sensitizers (see Figure 5b). This intermetallic distance was designed for approaching the critical radius for 50% efficiency in the Cr→Er energy transfer,[10] a situation which maximizes the Cr-centred ETU mechanism operating in the trinuclear CrErCr complex (Figure 7b, green trace).[11] Intermetallic communication *via* $Cr(^2E)\rightarrow Er(^4I_{9/2})$ energy transfer is indeed evidenced by the 20-50% reduction of the $Cr(^2E)$ excited lifetimes observed upon replacement of photophysically inactive Ln = Y (entries 1-2 in Table 1) with Ln = Er in CrLn and CrLnCr complexes (Figure S14).[11] Assuming that the Cr→Er energy transfer is the only source of additional quenching of the $Cr(^2E)$ excited state going from Ln = Y to Ln = Er, eq. (5) estimates the rate constants for $Cr(^2E)\rightarrow Er(^4I_{9/2})$ energy transfers, which amount to $W_1^{Cr\rightarrow Er} = 295(5)$ s^{-1} for CrEr and 170(4) s^{-1} for CrErCr at 10 K (entry 9 in Table 1 and Figure S15, τ_{Cr} stand for the characteristic lifetimes of the $Cr(^2E)$ levels measured in the various complexes).[11]

$$W_1^{\mathrm{Cr}\to\mathrm{Er}} = k_{\mathrm{Cr}}^{\mathrm{obs}}\left(\mathrm{Cr}_n\mathrm{Er}\right) - k_{\mathrm{Cr}}^{1\to0}\left(\mathrm{Cr}_n\mathrm{Y}\right) = \left[\tau_{\mathrm{Cr}}\left(\mathrm{Cr}_n\mathrm{Er}\right)\right]^{-1} - \left[\tau_{\mathrm{Cr}}\left(\mathrm{Cr}_n\mathrm{Y}\right)\right]^{-1} \tag{5}$$

Table 1 Characteristic excited state lifetimes (τ) and associated rate constants ($k = \tau^{-1}$) measured for [CrLn(**L1**)$_3$](CF$_3$SO$_3$)$_6$ and [CrLnCr(**L2**)$_3$](CF$_3$SO$_3$)$_9$ in the solid state at 10 K.[a]

	[CrLn(**L1**)$_3$]$^{6+}$	[CrLnCr(**L2**)$_3$]$^{9+}$
$\tau_{\mathrm{Cr}}^{1\to0}\left(\mathrm{Cr}_n\mathrm{Y}\right)$ /s	$2.767(10)\cdot10^{-3}$	$2.336(10)\cdot10^{-3}$
$k_{\mathrm{Cr}}^{1\to0}\left(\mathrm{Cr}_n\mathrm{Y}\right)$ /s^{-1}	362(1)	428(2)
$\tau_{\mathrm{Er}}^{1\to0}\left(\mathrm{Ga}_n\mathrm{Er}\right)$ /s	$4.28(2)\cdot10^{-6}$	$1.5(1)\cdot10^{-6}$
$k_{\mathrm{Er}}^{1\to0}\left(\mathrm{Ga}_n\mathrm{Er}\right)$ /s^{-1}	$2.34(1)\cdot10^{5}$	$6.7(4)\cdot10^{5}$
$\tau_{\mathrm{Er}}^{2\to0}\left(\mathrm{Ga}_n\mathrm{Er}\right)$ /s	$3.8(4)\cdot10^{-8}$	$4.0(2)\cdot10^{-8}$
$k_{\mathrm{Er}}^{\mathrm{obs}}\left(\mathrm{Ga}_n\mathrm{Er}\right)$ /s^{-1}	$2.6(3)\cdot10^{7}$	$2.5(1)\cdot10^{7}$
$k_{\mathrm{Er}}^{2\to0}\left(\mathrm{Ga}_n\mathrm{Er}\right)$ /s^{-1}	$1.615\cdot10^{3}$ [b]	$1.615\cdot10^{3}$ [b]
$k_{\mathrm{Er}}^{2\to1}\left(\mathrm{Ga}_n\mathrm{Er}\right)$ /s^{-1}	$2.6(3)\cdot10^{7}$ [c]	$2.5(1)\cdot10^{7}$ [c]
$W_1^{\mathrm{Cr}\to\mathrm{Er}}\left(\mathrm{Cr}_n\mathrm{Er}\right)$ /s^{-1}	295(5)	170(4)

[a] $k_{\mathrm{Cr}}^{1\to0}$, $k_{\mathrm{Er}}^{1\to0}$ and $k_{\mathrm{Er}}^{\mathrm{obs}}\left(\mathrm{Ga}_n\mathrm{Er}\right) = 1/\tau_{\mathrm{Er}}^{2\to0}\left(\mathrm{Ga}_n\mathrm{Er}\right) = k_{\mathrm{Er}}^{2\to1} + k_{\mathrm{Er}}^{2\to0}$ are the decay rate constants (i.e. the sum of radiative and non-radiative processes) of the Cr(^{2}E→^{4}A$_2$) transitions measured in Cr$_n$Y, and of the Er(^{4}I$_{13/2}$→^{4}I$_{15/2}$) and Er(^{4}S$_{3/2}$→^{4}I$_{15/2}$) transitions measured in Ga$_n$Er, respectively. $W_1^{\mathrm{Cr}\to\mathrm{Er}}$ are the rate constants for the Cr(^{2}E)→Er(^{4}I$_{9/2}$) energy transfer processes. [b] $k_{\mathrm{Er}}^{2\to0} = \left(\tau_{\mathrm{Er,rad}}^{^4\mathrm{S}_{3/2}}\right)^{-1}$ = (619 μs)$^{-1}$ is taken as the Er(^{4}S$_{3/2}$) radiative lifetime measured for Er^{3+}-doped into yttrium aluminium garnet.[21]
[c] $k_{\mathrm{Er}}^{2\to1}\left(\mathrm{Ga}_n\mathrm{Er}\right) = k_{\mathrm{Er}}^{\mathrm{obs}}\left(\mathrm{Ga}_n\mathrm{Er}\right) - k_{\mathrm{Er}}^{2\to0}$.

The resulting ETU mechanism proposed in Scheme 3 can be thus modelled with two simplified kinetic schemes (Figure 7).[20] As suggested by these diagrams, NIR irradiations into the Cr(^{2}E,^{2}T$_1$←^{4}A$_2$) transitions at $700 \leq \lambda_{\mathrm{exc}} \leq 750$ nm ($13330 \leq \tilde{\nu}_{\mathrm{exc}} \leq 14280$ cm^{-1}) indeed produced weak upconverted green emissions arising from the Er(^{4}S$_{3/2}$→^{4}I$_{15/2}$) transitions (Figure S16a), while the experimental slopes of 1.7-2.0 reported for the log-log plot of the upconverted intensity with respect to the incident laser intensities confirmed the successive absorption of two photons (Figure S16b).[11]

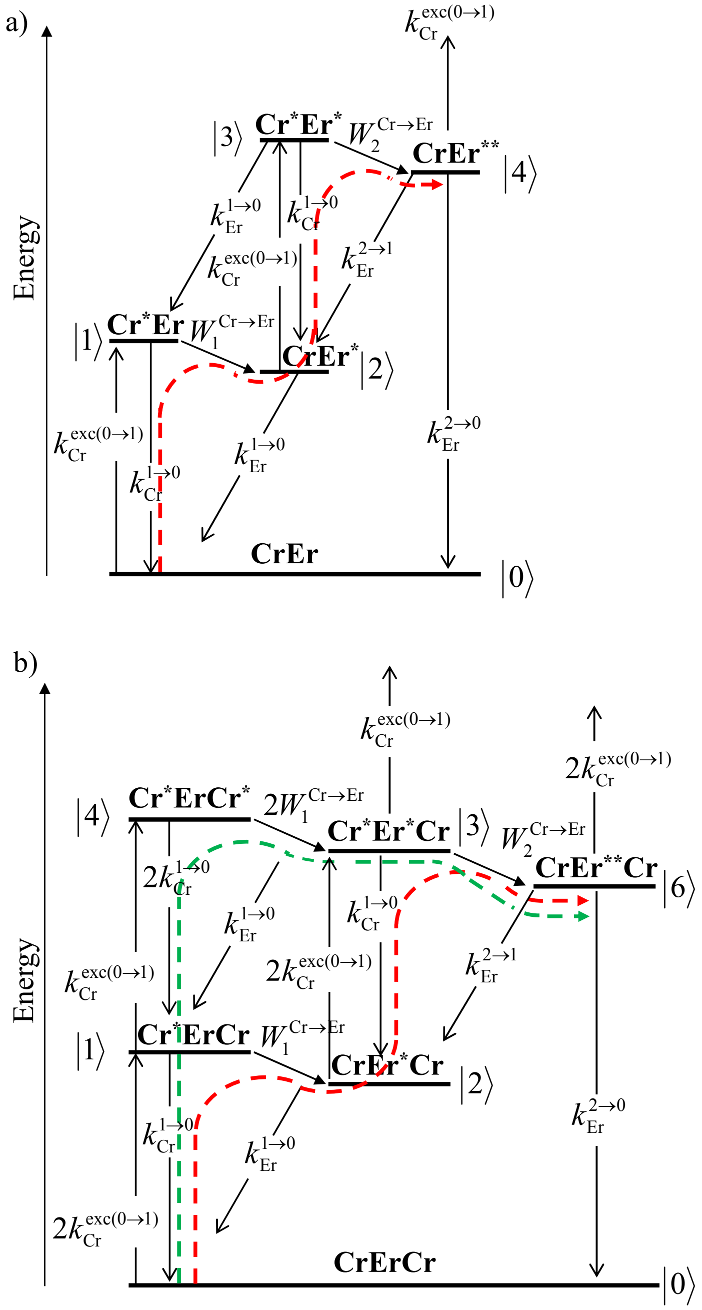

Figure 7 Simplified kinetic schemes[20] depicting the modelling of energy transfer upconversion (ETU) processes occurring upon off-resonance irradiation into the sensitizer-centred absorption bands in (a) the dinuclear $[CrEr(\mathbf{L1})_3]^{6+}$ and (b) the trinuclear $[CrErCr(\mathbf{L2})_3]^{9+}$ complexes. $k_{Cr}^{exc(0\to1)}$ is the pumping rate constant for irradiation into the $Cr(^2T_1 \leftarrow {}^4A_2)$ absorption band at $\lambda_p = 705$ nm (eq. 9). $k_{Cr}^{1\to0}$, respectively $k_{Er}^{1\to0}$, $k_{Er}^{2\to1}$ and $k_{Er}^{2\to0}$ are the decay rate constants (i.e. the sum of radiative and non-radiative processes) for the $Cr(^2E \to {}^4A_2)$ transition in Cr_nY and for the $Er(^4I_{13/2} \to {}^4I_{15/2})$, $Er(^4S_{3/2} \to {}^4I_{13/2})$ and $Er(^4S_{3/2} \to {}^4I_{15/2})$ transitions in Ga_nEr, respectively. $W_1^{Cr\to Er}$ and $W_2^{Cr\to Er}$ are the rate constants of Cr→Er energy transfer processes. The red dashed pathways highlight the Er-centred ETU mechanism, while the green dashed pathway holds for the additional Cr-centred ETU mechanism operating in Cr_nEr when $n \geq 2$.[11]

The complete set of kinetic rate constants collected in Table 1 allows us to further explore the ETU mechanisms operating in the dinuclear (Figure 7a) and trinuclear (Figure 7b) complexes. The macroscopic intensity measured for the final upconverted signal in CrEr and CrErCr is proportional to the normalized population density in the Er(^{4}S$_{3/2}$) excited state $N^{\left|\mathrm{Er}\left({}^4\mathrm{S}_{3/2}\right)\right\rangle}$ modulated by its intrinsic emission quantum yield $\phi_{\mathrm{lum}}^{\left|\mathrm{Er}\left({}^4\mathrm{S}_{3/2}\right)\right\rangle}$. The ratio of the upconverted intensities recorded for the two complexes under similar experimental conditions $I_{\mathrm{Er}}^{\mathrm{up}}\left(\mathrm{CrErCr}\right)/I_{\mathrm{Er}}^{\mathrm{up}}\left(\mathrm{CrEr}\right)$ thus obeys eq. (6).[11]

$$\frac{I_{\mathrm{Er}}^{\mathrm{up}}\left(\mathrm{CrErCr}\right)}{I_{\mathrm{Er}}^{\mathrm{up}}\left(\mathrm{CrEr}\right)}=\frac{N^{\left|\mathrm{Er}\left({}^4\mathrm{S}_{3/2}\right)\right\rangle}\left(\mathrm{CrErCr}\right)}{N^{\left|\mathrm{Er}\left({}^4\mathrm{S}_{3/2}\right)\right\rangle}\left(\mathrm{CrEr}\right)}\cdot\frac{\phi_{\mathrm{lum}}^{\left|\mathrm{Er}\left({}^4\mathrm{S}_{3/2}\right)\right\rangle}\left(\mathrm{CrErCr}\right)}{\phi_{\mathrm{lum}}^{\left|\mathrm{Er}\left({}^4\mathrm{S}_{3/2}\right)\right\rangle}\left(\mathrm{CrEr}\right)} \qquad (6)$$

Since the Er^{3+} cation is only slightly more accessible to high-energy vibrations in [CrEr(**L1**)$_3$]$^{6+}$ than in [CrErCr(**L2**)$_3$]$^{9+}$ (*vide supra*), one can reasonably assume that $\phi_{\mathrm{lum}}^{\left|\mathrm{Er}\left({}^4\mathrm{S}_{3/2}\right)\right\rangle}\left(\mathrm{CrErCr}\right) \approx \phi_{\mathrm{lum}}^{\left|\mathrm{Er}\left({}^4\mathrm{S}_{3/2}\right)\right\rangle}\left(\mathrm{CrEr}\right)$ and that therefore the ratio of intensities roughly corresponds to the ratio of the normalized population densities $N^{\left|\mathrm{Er}\left({}^4\mathrm{S}_{3/2}\right)\right\rangle}\left(\mathrm{CrErCr}\right)/N^{\left|\mathrm{Er}\left({}^4\mathrm{S}_{3/2}\right)\right\rangle}\left(\mathrm{CrEr}\right)$. Under Cr-centred excitation at a fixed incident pump intensity *P*, the pumping rate constant $k_{\mathrm{Cr}}^{\mathrm{exc}(0\to1)}$ is given by eq. (7), where λ_{p} is the pump wavelength, $\sigma_{\mathrm{Cr}}^{0\to1}$ is the absorption cross section of the Cr(^{2}E,^{2}T$_1$←^{4}A$_2$) transition, *h* is the Planck constant and *c* is the vacuum speed of light.[22]

$$k_{\mathrm{Cr}}^{\mathrm{exc}(0\to1)}=\frac{\lambda_{\mathrm{p}}}{hc}P\sigma_{\mathrm{Cr}}^{0\to1} \qquad (7)$$

Assuming that all the kinetic rate constants involved in the kinetic diagrams depicted in Figure 7 are at hand. The normalized population densities for each level can be computed with eq. (8), whereby ***M*** is the kinetic matrix associated to each kinetic diagram (Figures S17-S18).[11,17]

$$\left[\frac{dN^{|i\rangle}}{dt}\right]=\boldsymbol{M}\times\left[N^{|i\rangle}\right] \qquad (8)$$

The steady-state regime $dN^{|i\rangle}/dt = 0$ induced by the continuous-wave irradiation of the sensitizer reduces eq. (8) to $\boldsymbol{M} \times \left[N^{|i\rangle}\right] = 0$, a situation 'easily' solved for $\left[N^{|i\rangle}\right]$ by using eq. (9) where ***M'*** is the rectangular matrix produced by the inclusion of mass conservation $\sum_i N^{|i\rangle} = N_{\text{tot}} = 1$ into the square kinetic matrix ***M*** ($^{\text{T}}\boldsymbol{M'}$ is the transpose matrix, see Appendix 4 for mathematical details).[11]

$$\left[N^{|i\rangle}\right] = \left({}^{\text{T}}\boldsymbol{M'} \times \boldsymbol{M'}\right)^{-1} \times {}^{\text{T}}\boldsymbol{M'} \times \begin{bmatrix} 0 \\ \cdot \\ 0 \\ N_{\text{tot}} \end{bmatrix} \qquad (9)$$

The successive introduction of the rate constants gathered for [CrEr(**L1**)$_3$](CF$_3$SO$_3$)$_6$ and for [CrErCr(**L2**)$_3$](CF$_3$SO$_3$)$_9$ into eq. (9) provides the normalized population densities and their ratio $N^{|\text{Er}(^4\text{S}_{3/2})\rangle}(\text{CrErCr}) / N^{|\text{Er}(^4\text{S}_{3/2})\rangle}(\text{CrEr})$ so that the two experimentally non-accessible parameters, *i.e.*, the Cr(^{2}E,^{2}T$_1$←^{4}A$_2$) absorption cross sections $\sigma_{\text{Cr}}^{0\to1}$ required for computing $k_{\text{Cr}}^{\text{exc}(0\to1)}$ in eq. (7) and the rate constants for the second energy transfer process $W_2^{\text{Cr}\to\text{Er}}$ responsible for the Er(^{4}S$_{3/2}$←^{4}I$_{13/2}$) superexcitation pathway, can be estimated. Assuming that 1) $\sigma_{\text{Cr}}^{0\to1}(\text{CrEr}) \approx \sigma_{\text{Cr}}^{0\to1}(\text{CrErCr}) = 10^{-24}$ m^2,[23] and 2) the trend in energy transfer processes experimentally observed for $W_1^{\text{Cr}\to\text{Er}}$ also holds for $W_2^{\text{Cr}\to\text{Er}}$ (*i.e.* $W_2^{\text{Cr}\to\text{Er}}(\text{CrEr}) = W_1^{\text{Cr}\to\text{Er}}(\text{CrEr}) = 295$ s^{-1} and $W_2^{\text{Cr}\to\text{Er}}(\text{CrErCr}) = W_1^{\text{Cr}\to\text{Er}}(\text{CrErCr}) = 170$ s^{-1}), we calculated $N^{|\text{Er}(^4\text{S}_{3/2})\rangle}(\text{CrErCr}) / N^{|\text{Er}(^4\text{S}_{3/2})\rangle}(\text{CrEr}) \approx 10$ (Figure 8), in fair agreement with the experimental ratios of $I_{\text{Er}}^{\text{up}}(\text{CrErCr}) / I_{\text{Er}}^{\text{up}}(\text{CrEr}) = 4\text{-}10$ reported for the upconverted intensities measured for the two complexes in the 10-50 K range (Figure S16).[11] For large pump intensities (log(*P*) ≥ 1), the computed $I_{\text{Er}}^{\text{up}}(\text{CrErCr}) / I_{\text{Er}}^{\text{up}}(\text{CrEr})$ ratio takes a downturn due to saturation effects affecting the Cr-centred ETU mechanism in the triad (Figure 8b).

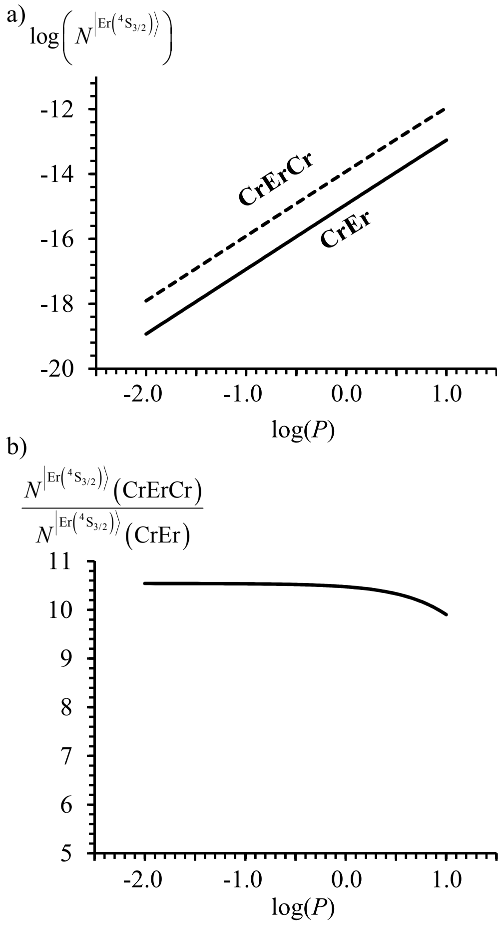

Figure 8 a) Log-log plot and b) ratio of the quadratic dependence of the steady-state normalized population densities $N^{|\mathrm{Er}(^4\mathrm{S}_{3/2})\rangle}$ on the incident pump intensity (P in W/mm^2) computed for the dinuclear [CrEr(**L1**)$_3$](CF$_3$SO$_3$)$_6$ (full trace) and for the trinuclear [CrErCr(**L2**)$_3$](CF$_3$SO$_3$)$_9$ (dotted trace) complexes using eq. (9) and the kinetic rate constants gathered in Table 1. $\sigma_{\mathrm{Cr}}^{0\to1}(\mathrm{CrEr}) \approx \sigma_{\mathrm{Cr}}^{0\to1}(\mathrm{CrErCr}) = 10^{-24}$ m^2,[23] $W_2^{\mathrm{Cr}\to\mathrm{Er}}(\mathrm{CrEr}) = W_1^{\mathrm{Cr}\to\mathrm{Er}}(\mathrm{CrEr}) = 295$ s^{-1} and $W_2^{\mathrm{Cr}\to\mathrm{Er}}(\mathrm{CrErCr}) = W_1^{\mathrm{Cr}\to\mathrm{Er}}(\mathrm{CrErCr}) = 170$ s^{-1} (see text).

Conclusion

This work demonstrates that the photophysically active and kinetically inert Cr$^{\mathrm{III}}$ cations found in dinuclear [CrLn(**L1**)$_3$]$^{6+}$ and trinuclear [CrLnCr(**L2**)$_3$]$^{9+}$ triple-stranded helicates can be replaced with the closed-shell Ga$^{\mathrm{III}}$ to give slightly less inert, isostructural [GaLn(**L1**)$_3$]$^{6+}$ and trinuclear [GaLnGa(**L2**)$_3$]$^{9+}$ complexes, for which the photophysical properties of the lanthanide cations can be deciphered without the complication due to the presence of the d-block cations. In this context, the pseudo-tricapped trigonal prismatic [ErN_9] chromophore appears to be exceptional in its capacity to simultaneously emits downshifted visible light arising from the Er($^4S_{3/2}$) level and near-infrared emission from the lowest Er($^4I_{15/2}$) excited level upon ligand-centred excitation, and this despite the presence of high-energy oscillators brought by the organic ligand strands. It is therefore not so surprising, but still remarkable, that the replacement of Er^{III} with either Tm^{III} (Figure S19) or Ho^{III} (Figure S20) in [GaLnGa(**L2**)$_3$]$^{9+}$ similarly produces rich lanthanide-centred luminescence upon UV-excitation of the aromatic receptor (Figure S21). The combination of the [ErN_9] chromophore, acting as the activator, with optically-adapted strong-field pseudo-octahedral [CrN_6] sensitizers in [CrEr(**L1**)$_3$]$^{6+}$ and [CrErCr(**L2**)$_3$]$^{9+}$ complexes further tolerates radiative visible de-excitation of the Er($^4S_{3/2}$) level and Cr-centred NIR excitation induces light-upconversion obeying an ETU mechanism (Scheme 3). Such behaviour requires a collection of favourable conditions which are difficult to gather in a single entity and, despite efficient Cr(^2E)→Tm($^3H_4$) energy transfer processes observed in [CrTmCr(**L2**)$_3$]$^{9+}$ (Figure S22), we were unable to detect chromium-to-thulium ETU (Figure S23), probably because the target blue Tm($^1G_4$→$^3H_6$) emission is quenched by an efficient Tm($^1G_4$)→Cr($^4T_2$) energy back-transfer (Figure S21). For [CrHoCr(**L2**)$_3$]$^{9+}$, the poor energy match between the Cr(^2E) and Ho($^5I_5$) levels (Figure S21) limits the Cr→Ho energy transfer rate constant to less than 100 s^{-1} (Figure S22), and no upconversion could either be evidenced upon Cr-centred excitation (Figure S24). Finally, numerical simulations using eq. (11) show that, using reasonable values for the various excited lifetimes in metallic sensitizers (in the millisecond range) and activators (in the microsecond range) involved in heterometallic M_nLn (supra)molecular complexes, both Ln-centred (red pathway in Figure 7) and M-centred (green pathway in Figure 7) ETU mechanisms greatly benefit from the maximization of (i) the number n of sensitizers per activator and (ii) the rate constants for the second M→Ln energy transfer process ($W_2^{\mathrm{M}\to\mathrm{Ln}}$). As a test, a unique and common value for the intermetallic Cr→Er energy transfer rates constants in the CrEr and CrErCr complexes was considered for comparison purpose. Introducing $W_2^{\mathrm{Cr}\to\mathrm{Er}}(\mathrm{CrEr})$ =

$W_1^{\mathrm{Cr\to Er}}(\mathrm{CrEr}) = W_2^{\mathrm{Cr\to Er}}(\mathrm{CrErCr}) = W_1^{\mathrm{Cr\to Er}}(\mathrm{CrErCr}) = 170\ \mathrm{s}^{-1}$ into eq. (9) yields $N^{|\mathrm{Er}(^4\mathrm{S}_{3/2})\rangle}(\mathrm{CrErCr})/N^{|\mathrm{Er}(^4\mathrm{S}_{3/2})\rangle}(\mathrm{CrEr}) \approx 220$ (Figure S25), a ratio which would have prevented the experimental detection of upconverted luminescence for the dinuclear CrEr helicate with our setup. The weak, but measurable upconverted signal experimentally recorded for the latter $[\mathrm{CrEr}(\mathbf{L1})_3]^{6+}$ complex upon chromium-centred NIR excitation is thus indebted to the Cr→Er rate constant, $W^{\mathrm{Cr\to Er}}$, which is twice as large as that measured in the trinuclear $[\mathrm{CrErCr}(\mathbf{L2})_3]^{9+}$ analogue. Further optimization should therefore focus on the increase of $W_2^{\mathrm{M\to Ln}}$ with the help of super-exchange mechanisms in polynuclear $\mathrm{M_nLn}$ complexes.[24]

Experimental

Solvents and starting materials.

These were purchased from Strem, Acros, Fluka AG and Aldrich and used without further purification unless otherwise stated. The trifluoromethanesulfonate salts $\mathrm{Ln(CF_3SO_3)_3}\cdot x\mathrm{H_2O}$ were prepared from the corresponding oxide (Aldrich 99.99%).[25] The synthesis of ligand **L1** is detailed in Appendix 1. The ligand **L2**[26] and the complexes $[\mathrm{MLn}(\mathbf{L1})_3](\mathrm{CF_3SO_3})_6\cdot x(\mathrm{H_2O})\cdot y(\mathrm{C_3H_5N})$ and $[\mathrm{MLnM}(\mathbf{L2})_3](\mathrm{CF_3SO_3})_9\cdot x(\mathrm{H_2O})\cdot y(\mathrm{C_3H_5N})$ were prepared according to literature procedures (M= Cr, Ga and Ln = Ho, Tm, Er, Y using propionitrile as a solvent) and characterized by elemental analyses (Table S1) and single-crystal X-ray diffraction.[11] Acetonitrile and dichloromethane were distilled over calcium hydride.

Spectroscopic and Analytical Measurements. The details of the setup and procedures used for recording high-resolution emission spectra at variable temperature under various excitation conditions were reported in ref. 11. Time-resolved luminescence spectra of $[\mathrm{GaEr}(\mathbf{L1})_3](\mathrm{CF_3SO_3})_6$ and $[\mathrm{GaErGa}(\mathbf{L2})_3](\mathrm{CF_3SO_3})_9$ were obtained from powder samples directly mounted onto copper plates using conductive silver glue, and cooled in an optical closed-cycle cryostat capable of reaching low temperatures down to 3 K in a helium atmosphere (*Sumitono SHI-950/Janis Research CCS-500/204*). High-resolution emission spectra were recorded upon excitation with Nd:YAG lasers (*Quantel Brilliant B*) by using the third harmonic at 355 nm. The laser was connected to a gated CCD detector (Andor iSTAR)during the monitoring of the luminescence spectra. The emitted light was analysed at 90° using an *Andor SR-163* monochromator (slits 100 μm) with a holographic grating (600 grooves/mm, blazed at 500 nm). Appropriate filters (395 or 435 nm cutoff) were used to remove residual excitation laser light, the Rayleigh scattered light and associated harmonics from the emission spectra. A kinetic series was recorded using a gate pulse width of 15 ns and scanning the delay from just before the arrival of the laser pulse to 350 ns in steps of 10 ns. Each spectrum corresponds to the sum of 1200-5000 scans. All the luminescence spectra were transferred to a PC for data analysis. The intensity at 541 nm and the integrated intensity between 535 and 560 nm corresponding to the Er($^4S_{3/2}\rightarrow{}^4I_{15/2}$) transition were calculated for each curve after background correction of the ligand-centred emission. The maximum intensity and the integrated intensity *vs* the time (0-350 ns) were plotted, from which the characteristic lifetimes for the Er($^4S_{3/2}$) level could be estimated. ^{1}H and ^{13}C NMR spectra were recorded at 293 K on a *Bruker Avance* 400 MHz spectrometer. Chemical shifts are given in ppm with respect to tetramethylsilane $Si(CH_3)_4$. Pneumatically-assisted electrospray (ESI) mass spectra were recorded from 10^{-4} M solutions on an Applied Biosystems API 150EX LC/MS System equipped with a Turbo Ionspray source®. Elemental analyses were performed by K. L. Buchwalder from the Microchemical Laboratory of the University of Geneva. Electronic absorption spectra in the UV-Vis were recorded at 20 °C from solutions with a Perkin-Elmer Lambda 900 spectrometer using quartz cells of 10 or 1 mm path length. The mathematical analyses were performed by using Igor Pro® (WaveMetrics Inc.) and Excel® (Microsoft) softwares.

X-Ray Crystallography. Fragile crystals of $[GaErGa(\mathbf{L2})_3](CF_3SO_3)_9(CH_3CN)_{35.5}$ (**16**) were obtained by slow diffusion of tert-butylmethylether into an acetonitrile solution of $[GaErGa(\mathbf{L2})_3]^{9+}$, while those of $[CrEr(\mathbf{L1})_3](CF_3SO_3)_6(C_3H_5N)_{26}$ (**17**) were obtained by the slow diffusion of tert-butylmethylether into a concentrated propionitrile solution of $[CrEr(\mathbf{L1})_3]^{6+}$. According that the crystals did not survive when separated from their mother liquors, we deposited the crystals on a filter paper, briefly sucked the excess solvent under vacuum and dissolved the resulting materials into CD_3CN. The ^1H NMR spectra showed the presence of the $[GaErGa(\mathbf{L2})_3]^{9+}$, resp. $[CrEr(\mathbf{L1})_3]^{6+}$ cations together with acetonitrile, resp. propionitrile molecules, but no signal for the heavy ether. It was therefore assumed that the crystals contained $[GaErGa(\mathbf{L2})_3](CF_3SO_3)_9$ and $[CrEr(\mathbf{L1})_3](CF_3SO_3)_6$ together with nitrile solvent molecules. Summary of crystal data, intensity measurements and structure refinements for $[GaErGa(\mathbf{L2})_3](CF_3SO_3)_9(CH_3CN)_{35}$ (**16**) and $[CrEr(\mathbf{L1})_3](CF_3SO_3)_6(C_3H_5N)_{26}$ (**17**) were collected in Tables S4 and S9 (Supporting Information). Each crystal was mounted on a kapton loop with protection oil. Cell dimensions and intensities were measured at 150 K on an Agilent Supernova diffractometer with mirror-monochromated Cu[Kα] radiation ($\lambda = 1.54187$) for **16** or at 100K using the Swiss-Norwegian beamlines, European Synchtron Radiation Facility (λ = 0.8231 Å) for **17**. Data were corrected for Lorentz and polarization effects and for absorption. The structure was solved by direct methods (SIR97),[27] all other calculations were performed with ShelX97[28] systems and ORTEP[29] programs. CCDC-1003567 and CCDC-1003568 contain the supplementary crystallographic data. The cif files can be obtained free of charge via www.ccdc.cam.ac.uk/conts/retrieving.html (or from the Cambridge Crystallographic Data Centre, 12 Union Road, Cambridge CB2 1EZ, UK; fax: (+ 44) 1223-336-033; or deposit@ccdc.cam.ac.uk).

WARNING. The quality of the diffraction data and their refinement is low due to considerable disorder. For **16**, twelve triflates anions could be located and refined, but the absence of features that could be unambiguously attributed to the missing six triflates anions and to the solvent molecules in the Fourier difference map forced us to apply the Squeeze/bypass method (program PLATON) in order to take care of the remaining electronic density. There is a huge void in the structure, in which 2003 electrons per formula unit were attributed by squeeze. This corresponded to six triflates together with 71 acetonitrile molecules which were included in the unit cell. In **17**, the six $CF_3SO_3^-$ counter-anions and interstitial solvent molecules were highly disordered in large voids in the structure. In absence of diagnostic features in the Fourier difference map, the

Squeeze/bypass method (program PLATON)[30] was used to take care of the remaining electron density, which was eventually assigned to six triflates and 26 propionitrile molecules. (details are given in the associated CIF file).

Supporting Information

Synthesis of ligand **L1** (Appendix 1), determination of thermodynamic exchange constants (Appendix 2), kinetic analysis (Appendix 3) and calculation of normalized steady-state population densities (Appendix 4). Tables collecting elemental analysis (Table S1), ESI-MS peaks (Tables S2-S3) and crystallographic data (Tables S4-S5). Figures showing NMR spectra (Figures S1-S4), ORTEP views (Figure S5), packing interactions (Figure S6-S8) and photophysical data (Figures S9-S25).

Acknowledgements

This work was supported through grants from the Swiss National Science Foundation (grant numbers 200020_140222 and 200020-125175), the University of Geneva (INNOGAP), la Ligue contre le Cancer and the Institut National de la Santé et de la Recherche Médicale (INSERM). The work was carried out within the COST Actions TD1004 and CM1006.

References and notes

1 (a) D. S. Chemla and J. Zyss (Eds.), *Nonlinear Optical Properties of Organic Molecules and Crystals*, Academic Press, Orlando,1987. (b) P. N. Prasad and D. J. Williams, *Introduction to Nonlinear Optical Effects in Molecules and Polymers*, John Wiley & Sons, Inc., New York, 1991. (c) J. Zyss, *Molecular Nonlinear Optics: Materials, Physics and Devices*, Academic Press, Boston, 1994. (d) H.S. Nalwa and S. Miyata (Eds.), *Nonlinear Optics of Organic Molecules and Polymers*, CRC Press, Boca Raton, 1997.

2 F. Terenziani, C. Katan, E. Badaeva, S. Tretiak and M. Blanchard-Desce, *Adv. Mater.* 2008, **20**, 4641-4678. (a) C. Andraud and O. Maury, *Eur. J. Inorg. Chem.*, 2009, 4357-4371. (b) P. Neveu, D. K. Sinha, P. Kettunen, S. Vriz, L. Jullien and D. Bensimon, *Springer Series in Chemical Physics* 2010, **96**, 305-316. (c) A. D'Aléo, A. Bourdolle, S. Brustlein, T. Fauquier,

A. Grichine, A. Duperray, P. L. Baldeck, C. Andraud, S. Brasselet and O. Maury, *Angew. Chem. Int. Ed.*, 2012, **51**, 6622-6625.

3 (a) S. V. Eliseeva and J.-C. G. Bünzli, *New J. Chem.*, 2011, **35**, 1165-1176. (b) X. Huang, S. Han, W. Huang and X. Liu, *Chem. Soc. Rev.*, 2013, **42**, 173-201. (c) J.-C. G. Bünzli and A.-S. Chauvin, in *Handbook on the Physics and Chemistry of Rare Earths*, eds. J.-C. G. Bünzli and V. K. Pecharsky, Elsevier North Holland, Amsterdam, 2014, vol. 44, pp. 169-281.

4 (a) T. N. Singh-Rachford and F. N. Castellano, *Coord. Chem. Rev.*, 2010, **254**, 2560-2573. (b) J. Zhao, S. Ji and H. Guo, *RSC Adv.*, 2011, **1**, 937-950. (c) A. Monguzzi, R. Tubino, S. Hoseinkhani, M. Campione and F. Meinardi, *Phys. Chem. Chem. Phys.*, 2012, **14**, 4322-4332. (d) , J.-H. Kim, F. Deng, F. N. Castellano and J.-H. Kim *Chem. Mater.* **2012**, *24*, 2250-2252. (e) X. Huang, S. Han, W. Huang and X. Liu, *Chem. Soc. Rev.* **2013**, *42*, 173-201.

5 (a) F. Auzel, *Chem. Rev.*, 2004, **104**, 139-173. (b) B. M. van der Ende, L. Aarts and A. Meijerink, *Phys. Chem. Chem. Phys.*, 2009, **11**, 11081-11095. (c) M. Haase and H. Schäfer, *Angew. Chem. Int. Ed.*, 2011, **50**, 5808-5829.

6 L. Aboshyan-Sorgho, M. Cantuel, S. Petoud, A. Hauser and C. Piguet, *Coord. Chem. Rev.*, 2012, **256**, 1644-1663.

7 C. Reinhard and H. U. Güdel, *Inorg. Chem.*, 2002, **41**, 1048-1055.

8 O. A. Blackburn, M. Tropiano, T. J. Sorensen, J. Thom, A. Beeby, L. M. Bushby, D. Parker, L. S. Natrajan and S. Faulkner, *Phys. Chem. Chem. Phys.*, 2012, **14**, 13378-13384.

9 H. Suzuki, Y. Nishida and S. Hoshino, *Mol. Cryst. Liq. Cryst.*, 2003, **406**, 27/[221]-237/[231].

10 L. Aboshyan-Sorgho, C. Besnard, P. Pattison, K. R. Kittilstved, A. Aebischer, J.-C. G. Bünzli, A. Hauser and C. Piguet, *Angew. Chem. Int. Ed.*, 2011, **50**, 4108-4112.

11 Y. Suffren, D. Zare, S. V. Eliseeva, L. Guénée, H. Nozary, T. Lathion, L. Aboshyan-Sorgho, S. Petoud, A. Hauser and C. Piguet, *J. Phys. Chem. C*, 2013, **117**, 26957-26963.

12 (a) G. A. Kumar, R. Riman, S. C. Chae, Y. N. Jang, I. K. Bae and H. S. Moon, *J. Appl. Phys.*, 2004, **95**, 3243-3249. (b) A. K. Singh, S. B. Rai, D. K. Rai and V. B. Singh, *Appl. Phys. B*, 2006, **82**, 289-294. (c) F. Prudenzano, L. Mescia, L. Allegretti, V. Moizan, V. Nazabal and F. Smektala, *Optical Materials*, 2010, **33**, 241-245.

13 (a) J. W. Hofstraat, M. P. Oude Wolbers, F. C. J. M. Van Veggel, D. N. Reinhoudt, M. H. V. Werts and J. W. Verhoeven, *J. Fluoresc.*, 1998, **8**, 301-308. (b) M. P. Oude Wolbers, F. C. J. M. van Veggel, F. G. A. Peters, E. S. E. van Beelen, J. W. Hofstraat, F. A. J. Geurts and D. N. Reinhoudt, *Chem. Eur. J.*, 1998, **4**, 772-780. (c) L. H. Sloof, A. Polman, M. P. O. Wolbers, F. C. J. M. van Veggel, D. N. Reinhoudt and J. W. Hofstraat, *J. Appl. Phys.*, 1998, **83**, 497-503. (d) B. M. Flanagan, P. V. Bernhardt, E. R. Krausz, S. R. Lüthi and M. J. Riley, *Inorg. Chem.*, 2001, **40**, 5401-5407. (e) K. Kuriki, Y. Koike and Y. Okamoto, *Chem. Rev.*, 2002, **102**, 2347-2356. (f) L. H. Sloof, A. van Blaaderen, A. Polman, G. A. Hebbink, S. I. Klink, F. C. J. M. Van Veggel, D. N. Reinhoudt and J. W. Hofstraat, *J. Appl. Phys.*, 2002, **91**, 3955-3980. (g) V. S. Sastri, J.-C. Bünzli, V. R. Rao, G. V. S. Rayudu nd J. R. Perumareddi *Modern Aspects of Rare Earths and Their Complexes*, Elsevier, Amsterdam, 2003, chap 8, pp 629-632. (h) S. Quici, G. Marzanni, A. Forni, G. Accorsi and F. Barigelletti, I*norg. Chem.*, 2004, **43**, 1294-1301. (i) G. M. Davies, H. Adams, S. J. A. Pope, S. Faulkner and M. D. Ward, *Photochem. Photobiol. Sci.*, 2005, **4**, 829-834. (j) G. Mancino, A. J. Ferguson, A. Beeby, N. J. Long and T. S. Jones, *J. Am. Chem. Soc.*, 2005, **127**, 524-525.(k) J. B. Oh, Y. H. Kim, M. K. Nah and H. K. Kim, *J. Lumin.*, 2005, **111**, 255-264. (l) M.-K. Nah, H.-G. Cho, H.-J. Kwon, Y.-J. Kim, C. Park, H. K. Kim and J.-G. Kang, *J. Phys. Chem. A*, 2006, **110**, 10371-10374. (m) S. Destri, M. Pasini, W. Porzio, F. Rizzo, G. Dellepiane, M. Ottonelli, G. Musso, F. Meinardi and L. Veltri, J. Luminesc., 2007, **127**, 601-610. (n) X. Li, Z. Si, C. Pan, L. Zhou, Z. Li, X. Li, J. Tang and H. Zhang, *Inorg. Chem. Commun.*, 2009, **12**, 675-677. (o) F. Artizzu, M. L. Mercuri, A. Serpe and P. Deplano, *Coord. Chem. Rev.*, 2011, **255**, 2514-2529. (p) D. J. Lewis, F. Moretta, A. T. Holloway and

Z. Pikramenou, *Dalton Trans.*, 2012, **41**, 13138-13146. (q) P. Martin-Ramos, C. Coya, A. L. Alvarez, M. Ramos Silva, C. Zaldo, J. A. Paixao, P. Chamorro-Posada and J. Martin-Gil, *J. Phys. Chem. C*, 2013, **117**, 10020-10030.

14 (a) C. Piguet, J.-C. G. Bünzli, G. Bernardinelli and A. F. Williams, *Inorg. Chem.*, 1993, **32**, 4139-4149. (b) C. Piguet, J.-C. G. Bünzli, G. Bernardinelli, C. G. Bochet and P. Froidevaux, *J. Chem. Soc., Dalton Trans.*, 1995, 83-97. (c) S. Petoud, J.-C. G. Bünzli, F. Renaud, C. Piguet, K. J. Schenk and G. Hopfgartner, *Inorg. Chem.*, 1997, **36**, 5750-5760.

15 (a) C. Piguet, E. Rivara-Minten, G. Hopfgartner and J.-C. G. Bünzli, *Helv. Chim. Acta*, 1995, **78**, 1541-1566. (b) C. Piguet, J.-C. G. Bünzli, G. Bernardinelli, G. Hopfgartner, S. Petoud and O. Schaad, *J. Am. Chem. Soc.*, 1996, **118**, 6681-6697.

16 D. Lavabre, V. Pimienta, G. Levy and J. C. Micheau, *J. Phys. Chem.*, 1993, **97**, 5321-5326.

17 M. E. Starzak, *Mathematical Methods in Chemistry and Physics*, Plenum press New York, pp 289-357 (1989).

18 Because of the intense visible luminescence of $[GaEuGa(\mathbf{L2})_3](CF_3SO_3)_9$, the Er salts used for preparing $[GaErGa(\mathbf{L2})_3](CF_3SO_3)_9$ must have the highest possible purity. In our hands, Er_2O_3 (99.99%) provided the emission spectrum depicted in Figure 5 (blue trace), but the use of Er_2O_3 (99.9%) showed concomitant Er- and Eu-centred emissions at low temperature (Figure S10b).

19 O. S. Wenger, H. Güdel and S. Kück, *J. Chem. Phys.*, 2002, **117**, 909-913.

20 For the sake of clarity, the kinetic diagrams collected in Figure 7 are limited to the lower excited states involved for two successive Cr-centred excitations. However, all calculations take into account the complete schemes described in ref. 11, which are reproduced in Figures S17a-S18a for the convenience of the reader.

21 S. Georgescu and V. Lupei, *J. Quantum. Elec.*, 1998, **34**, 1031-1040.

22 M. Pollnau, D. R. Gamelin, S. R. Lüthi and H. U. Güdel, *Phys. Rev.*, 2000, **B61**, 3337-3346.

23 The absorption cross section $\sigma^{i\to j}$ (in cm^2) is related to the molar extinction coefficient $\varepsilon^{i\to j}$ (in M^{-1}cm^{-1}) by using $\sigma^{i\to j} = 3.8\cdot 10^{-21}\cdot \varepsilon^{i\to j}$. Typical values of σ_{Cr} ≈ 10^{-24} m^2 have been reported in ref. 19 for the Cr($^2T_1$,$^2E \leftarrow {}^4A_2$) transitions observed for Cr^{3+} doped in $Cs_2NaScCl_6$.

24 M. E. von Arx, E. Burattini, A. Hauser, L. van Pieterson, R. Pellaux and S. Decurtins, *J. Phys. Chem. A*, 2000, **104**, 883-893.

25 J. F. Desreux, *Lanthanide Probes in Life, Chemical and Earth Sciences*; G. Choppin and J.-C. G. Bünzli (Eds), Elsevier: Amsterdam, chap 2 (1989).

26 C. Piguet, B. Bocquet and G. Hopfgartner, *Helv. Chim. Acta*, 1994, **77**, 931-942.

27 A. Altomare, M. C. Burla, M. Camalli, G. Cascarano, C. Giacovazzo, A. Guagliardi, G. Moliterni, G. Polidori and R. Spagna, *J. Appl. Cryst.*, 1999, **32**, 115-119.

28 G. M. Sheldrick, SHELXL97 Program *for the Solution and Refinement of Crystal Structures*, University of Göttingen, Germany, 1997.

29 ORTEP3 for Windows. L. J. Farrugia, *J. Appl. Crystallogr.*, 1997, **30**, 565.

30 P. Van der Sluis and A. L. Spek, *Acta Cryst.*, 1990, **A46,** 194-201.

Graphical content entry:

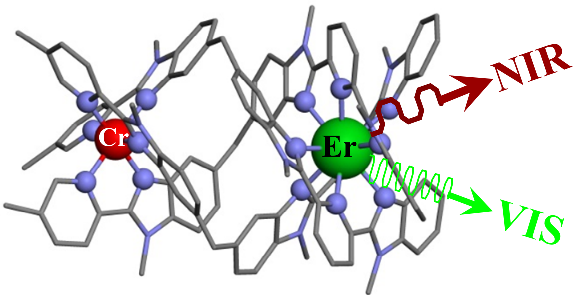

An unprecedented molecular [ErN_9] chromophore emits simultaneous dual green (542 nm) and near-infrared (1540 nm) light upon indirect excitation either via the polyaromatic strands (UV-to-Visible downshifting) or via the [CrN_6] sensitizer (NIR-to-Visible upconversion).